# Complete photoionization experiments via ultra-fast coherent control with polarization-multiplexing

P. Hockett*
*National Research Council of Canada, 100 Sussex Drive, Ottawa, K1A 0R6, Canada*

M. Wollenhaupt
*Institut für Physik, Carl von Ossietzky Universität Oldenburg, Carl-von-Ossietzky-Straße 9-11, 26129 Oldenburg, Germany*

C. Lux and T. Baumert
*Institut für Physik, Universität Kassel, Heinrich-Plett-Str. 40, 34132 Kassel, Germany*
(Dated: 23rd Feb. 2014)

Photoelectron angular distributions (PADs) obtained from ionization of potassium atoms using moderately intense femtosecond IR fields ($\sim 10^{12}$Wcm$^{-2}$) of various polarization states are shown to provide a route to "complete" photoionization experiments. Ionization occurs by a net 3-photon absorption process, driven via the $4s \rightarrow 4p$ resonance at the 1-photon level. A theoretical treatment incorporating the intra-pulse electronic dynamics allows for a full set of ionization matrix elements to be extracted from 2D imaging data. 3D PADs generated from the extracted matrix elements are also compared to experimental, tomographically reconstructed, 3D photoelectron distributions, providing a sensitive test of their validity. Finally, application of the determined matrix elements to ionization via more complex, polarization-shaped, pulses is demonstrated, illustrating the utility of this methodology towards detailed understanding of complex ionization control schemes and suggesting the utility of such "multiplexed" intra-pulse processes as powerful tools for measurement.

arXiv:1403.3315v1 [physics.atom-ph] 13 Mar 2014

So-called "complete" measurements of ionization dynamics aim to obtain the amplitudes and phases of the ionization matrix elements which describe the ionization event in terms of the partial wave decomposition of the outgoing photoelectron [1, 2]. Since determining the phases requires an observable in which interferences between partial waves are present, photoelectron angular distributions (PADs) are required for complete measurements. Such experiments have long been performed for atomic systems [1, 3] where, for example, PADs obtained via pump-probe schemes utilising linearly polarized light and a range of pump-probe geometries [4–6], or different polarization states [7], have allowed the relative amplitude and phase of two ionization matrix elements to be determined [8]. For molecules, various experimental techniques, including molecular frame PADs [9–11], time-resolved rotational wavepacket studies [12, 13] and state-resolved measurements [14–16], have been demonstrated. The common thread to all of these measurements is the necessity of a data-set containing sufficient information to reliably obtain the set of ionization matrix elements (which may be large) via some type of fitting procedure. Here "sufficient" refers to both the size of the experimental data-set and the fundamental level of detail present [2]. For example, measurements from the Zare group demonstrated the level of detail obtainable from experiments with linear and elliptically polarized light [14, 15]; work from Elliott's group investigated the role of interferences between 1 and 2 photon ionization pathways, including control of PADs [17, 18].

Control experiments have garnered much interest over the last 20 years, in particular with the aim of controlling the outcome of chemical reactions, as well as control over observables such as PADs [18–22]. Control experiments utilizing shaped laser pulses can also be considered as intra-pulse pump-probe experiments; in this context, such experiments may be highly-multiplexed, and could be considered as a natural continuation of (serial) frequency-domain schemes for measuring atomic and molecular properties. Furthermore, measurement of the relevant physical properties allows the control processes to be understood in detail, rather than treated as a black-box optimization scheme, as pointed out in refs. [23, 24]. In this work we demonstrate this principle using an experimental scheme originally designed with the aim of controlling PADs [20, 22] but, instead, make use of the data - measured as a function of polarization state - to elucidate the ionization matrix elements. Because of the high information content of the PADs obtained, four experimental measurements prove sufficient for a determination of the ionization matrix elements. The treatment can readily be extended to more complex, arbitrarily shaped pulses, and also to molecular ionization in cases where the intra-pulse dynamics is computationally tractable, allowing for truly multiplexed measurements beyond the proof-of-concept shown here. We demonstrate this principle by application of the determined matrix elements to ionization via a polarization-multiplexed pulse.

The experimental set-up has been covered in detail in refs. [20, 21, 25]. Here we briefly outline the control scheme for the case of polarization shaped pulses. Moderately intense ($\sim 10^{12}$ Wcm$^{-2}$) laser pulses (795 nm, 30 fs, bandwidth 60 meV FWHM) were generated by a Ti:Sapphire multi-pass amplifier. Basic control of the ellipticity of the pulse was achieved via a $\lambda/4$ plate, while more complex pulse shapes were attained with the use of a spatial light modulator in a $4f$ configuration [20, 26]. The laser pulses were focussed into potassium vapour generated by a dispenser source in the interaction region of a velocity-map

imaging spectrometer. The detector consisted of a dual-MCP stack, phosphor screen and CCD camera, allowing measurement of 2D projections of the full 3D photoelectron distribution. In the case of cylindrically symmetric distributions, a single 2D projection is sufficient to reconstruct the full 3D distribution via standard inversion techniques [**?** ]; for non-cylindrically symmetric distributions projections at several different angles to the detector must be obtained, and a tomographic reconstruction technique applied to obtain the original 3D distribution [25, 28, 29].

In order to understand and treat the *intra*-pulse light-matter interaction (i.e. simultaneous excitation and ionization dynamics) we split the problem conceptually into two steps, (1) a non-perturbative absorption at the 1-photon level, the "pump" step, (2) a perturbative 2-photon ionization, the "probe" step [30]. This is essentially an *intra*-pulse 1+2 REMPI (resonance-enhanced multi-photon ionization) scheme, where the first step is near-resonant with the potassium $4s \rightarrow 4p$ transition (which carries significant oscillator strength), and the second step is non-resonant. A schematic of the ionization pathways for this net 3-photon absorption process is given in figure 1(upper panel).

The "pump" process describes the interaction of the control field with the atom at the 1-photon level. With a moderately intense, near resonant field, Rabi oscillations are driven. These oscillations follow the driving electric field and, crucially, depend sensitively on the instantaneous properties of the light field, such as the polarization state and the frequency spread. The population dynamics during the laser pulse are then given by the time-dependent Schrödinger equation:

$$\frac{d}{dt}\begin{pmatrix} s(t) \\ p_{+1}(t) \\ p_{-1}(t) \end{pmatrix} = i \begin{pmatrix} 0 & \frac{1}{2}\Omega_L^*(t) & \frac{1}{2}\Omega_R^*(t) \\ \frac{1}{2}\Omega_L(t) & \delta_{+1} & 0 \\ \frac{1}{2}\Omega_R(t) & 0 & \delta_{-1} \end{pmatrix} \begin{pmatrix} s(t) \\ p_{+1}(t) \\ p_{-1}(t) \end{pmatrix} \tag{1}$$

where $s(t)$, $p_{+1}(t)$ and $p_{-1}(t)$ are the state vector components for the $4s$ and $4p(m = \pm 1)$ states; $\Omega_{L/R}(t) = \mu_{L/R} E_{L/R}(t)$ are Rabi frequencies, where $\mu_{L/R}$ are the transition amplitudes, and $E_{L/R}(t)$ represents the electric field expanded in a spherical basis; $\delta_{\pm 1}$ represents the detuning of the laser from the resonant frequency of the transition. In this work $\mu_{L/R}$, $E_0$ (total electric field strength) and $\hbar$ are all set to unity. For determination of PADs these simplifications are acceptable as only the *relative* population of $m = \pm 1$ states will affect the angular distribution [31]. In this case the relative populations are dependent only on the driving laser field polarization; in a case where additional $|l, m\rangle$ states are accessed, more careful treatment of the transition amplitudes $\mu_{L/R}$ would be required. An example of the population dynamics is given in figure 1(lower panel), illustrating how the difference in magnitudes of the $E_L(t)$ and $E_R(t)$ laser field components describing an elliptically polarized field give rise to different $p_{+1}$ and $p_{-1}$ populations.

The "probe" process describes the subsequent absorption of 2 photons resulting in ionization of the $4p$ excited state. By treating this step pertubatively the resultant matrix ele-

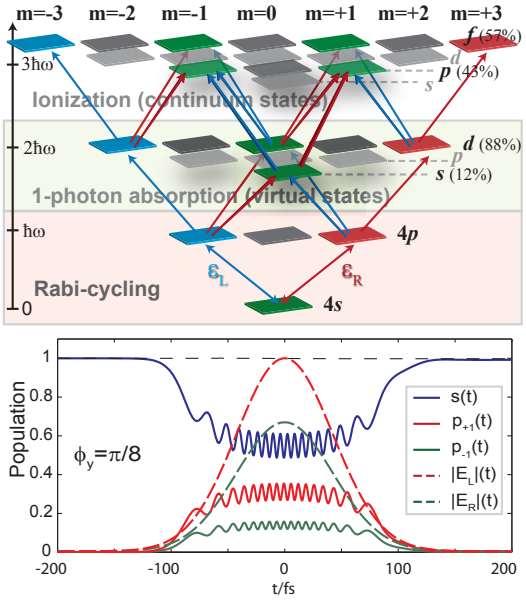


Figure 1. Schematic of the 3-photon ionization scheme for potassium. $|l, m\rangle$ states coloured red or blue are accessed by $E_R$ or $E_L$ components of the field only, while states coloured green can be accessed by both components via different pathways. States coloured dark grey are inaccessible $m$ levels within a populated $l$ manifold, while light grey states show inaccessible $l$ manifolds. Percentages give the $m$-summed weightings of the $l$ states as determined from the fitted radial matrix elements, as listed in table I; the continuum state populations are also summed over all paths, see main text for details. The lower panel shows an example of the population dynamics, in this case for an elliptically polarized pulse $\phi_y = \pi/8$, where $\phi_y$ is the spectral phase applied to the $y$-component of the $E$-field and is used to define polarization states throughout this work [20]; the envelope of the laser pulse is also shown in terms of the $E_L(t)$ and $E_R(t)$ components. Due to the detuning of the frequency of the laser pulse with respect to the atomic transition the time evolution of the population is characterized by coherent population return rather than Rabi oscillations.

ments are independent of the instantaneous pulse intensity, hence are assumed to be constant over the pulse envelope. In the perturbative regime, the 2-photon dipole transition amplitude for a transition from state $|l_i, m_i\rangle$ to a final state $|l_f, m_f\rangle$, via a virtual intermediate state $|l_v, m_v\rangle$, integrated over the pulse duration, can be written as:

$$d_{l_f m_f}(k) = \int d_{i\rightarrow v}(k,t) d_{v\rightarrow f}(k,t) dt = \int dt \sum_{\substack{l_i, m_i; l_v, m_v \\ q, q'}} R_{l_v l_f}(k) \langle l_f m_f, 1q' | l_v m_v \rangle R_{l_i l_v}(k) \langle l_v m_v, 1q | l_i m_i \rangle E_{q'}(t) E_q(t) p_{m_i}(t) \tag{2}$$

where the summation is over all pathways from the initial, ionizable, states $|l_i, m_i\rangle$, weighted by their populations $p_{m_i}(t)$, and all polarization states $q$. Here $R_{l_i l_f}(k)$ are the radial components and $\langle l_f m_f, 1q|l_i m_i\rangle$ are Clebsch-Gordan coefficients which describe the angular momentum coupling; the photoelectron kinetic energy dependence on time, given as $e^{i\delta\omega_e t}$ in ref. [20], has been omitted. This term is identical for all $|l, m\rangle$ channels, so will not affect the PADs in the case of polarization shaped pulses. We have assumed that the angular part of both bound-virtual and virtual-free transitions can be be described by matrix elements of the same form; we furthermore assume a single active electron picture with no angular momentum coupling of the virtual and final one-electron states to the nascent ion core. In general both of these simplifications could be removed, resulting in a more complex angular momentum coupling scheme and, possibly, more partial wave components due to additional electron-ion scattering.

The observed photoelectron yield as a function of angle, for a single $k$ or small energy range $dk$ over which we assume the $R(k)$ can be regarded as constant, is then given by the coherent square over all final (photoelectron) states:

$$I(\theta, \phi;\, k) = \sum_{\substack{l_f, m_f \\ l_f^{'}, m_f^{'}}} d_{l_f m_f}(k) Y_{l_f m_f}(\theta, \phi) d^*_{l_f^{'} m_f^{'}}(k) Y^*_{l_f^{'} m_f^{'}}(\theta, \phi) \quad (3)$$

where the $Y_{lm}(\theta, \phi)$ are spherical harmonics which describe the angular form of the photoelectron partial waves.

Finally, we note that the PAD can also be described phenomenologically by $\beta_{LM}$ parameters [1], where:

$$I(\theta, \phi;\, k) = \sum_{L,M} \beta_{LM}(k) Y_{LM}(\theta,\, \phi) \quad (4)$$

The information content of the observed PADs can be considered in terms of the number of $L$, $M$ terms present in this expansion, which will therefore depend on both the inherent properties of the system and the laser pulse parameters, as shown in equation 2. For example, use of linearly polarized light restricts eqn. 4 to terms with $M = 0$ only.

In the preceding treatment the angular momentum coupling is calculated analytically, and the population dynamics numerically; in both cases these computations are somewhat routine and are expected to be accurate. Therefore, only the $R_{ll}$ remain as unknowns: determination of these complex radial matrix elements is the aim of "complete" photoionization experiments. To generate distributions to compare with the experimental results, PADs calculated according to equation 3 were convoluted with a Gaussian radial distribution (defined in energy space) to generate gridded volumetric data; 2D image-plane projections were generated by summation of the 3D distributions. Although numerically intensive, this procedure generates 2D projections that can be compared directly with the 2D experimental imaging data even in the case of non-cylindrically symmetric distributions. In order to determine the $R_{ll}$, fitting to the experimental data was carried out to optimize the computed 2D projections. In this procedure the $R_{ll}$ were expressed in magnitude and phase form, $R_{ll} = |R_{ll}|e^{i\delta_{ll}}$, where $-\pi \leq \delta_{ll} \leq \pi$; also $R_{l_1 l_2} = R^*_{l_2 l_1}$. Because absolute phases cannot be determined, $\delta_{01}$ at the 1-photon level was set to zero as a reference phase. Technical details of this procedure will be given in a future publication [**?** ].

The best fit images are shown in figure 2(a)-(d). The fitted results show a reasonable agreement with the experimental data in terms of the form of the angular distributions, and trend with polarization, but less satisfactory agreement in terms of the width and scaling of the features. For the elliptically polarized cases this is not too surprising, as the polarization states used are only approximate. The linear and circularly polarized cases show a better, but still imperfect, agreement with the data; this is attributed to the assumption of a Gaussian radial distribution. Nonetheless, the obtained ionization matrix elements appear to be relatively insensitive to these issues because they are primarily defined by the angular coordinate of the image. The calculated $\beta_{LM}$, as a function of $\phi_y$, are shown in figure 2(e). Non-zero values are found for $L = 0$, 2, 4, 6 and even $M$ terms, consistent with the experimental symmetry and the total number of photons absorbed [1], and a smooth variation in the parameters is observed with ellipticity.

The fitted parameters obtained are given in table I. Here the magnitudes are normalized to give total cross-sections of unity at the 1-photon and 2-photon level. The results show that the final photoelectron wavefunction, summed over all paths to each final state $|R_{l_i l_f}|^2 = (\sum_v |R_{l_i l_v}||R_{l_v l_f}|)^2$, is 57% $f$-wave and 43% $p$-wave in character. This is consistent with the expectation from the shape of the PAD, which has strong $L = 6$ character, that the $f$-wave dominates, but also reveals a significant contribution from $l = 1$ partial waves, primarily via the $p \rightarrow s \rightarrow p$ channel. The relative phases of the final continuum waves are quite different, revealing partially destructive interference between the $p$ and $f$-waves. It is interesting to note that since the scattering phase and Wigner delay are directly related [32], these phase differences indicate a significant difference in emission time of all the continuum waves, including a dependence on the virtual state since the $p \rightarrow s \rightarrow p$ and $p \rightarrow d \rightarrow p$ paths accumulate different total phases [33].

To further validate these results we next consider in detail the full 3D distributions. Figure 3 shows the 3D photoelectron distributions for two polarization states. The experimental data, fig. 3(a) & (c), was tomographically reconstructed from a set of 2D images, as detailed in ref. [25]. The tomographic data provides a full 3D map of the PADs, providing details which may be obscured in single 2D projections of non-cylindrically symmetric distributions. This data compares well to the calculated distributions, fig. 3(b) & (d), with $R_{ll}$ based only on fitting of the less detailed 2D projections, confirming that the full angular structure is well-determined by the fitted matrix elements. The fit results were further validated at the level of the $\beta_{LM}$ parameters, extracted as a function of radius, from the tomographic data (eqn. 4); this analysis will be discussed in a

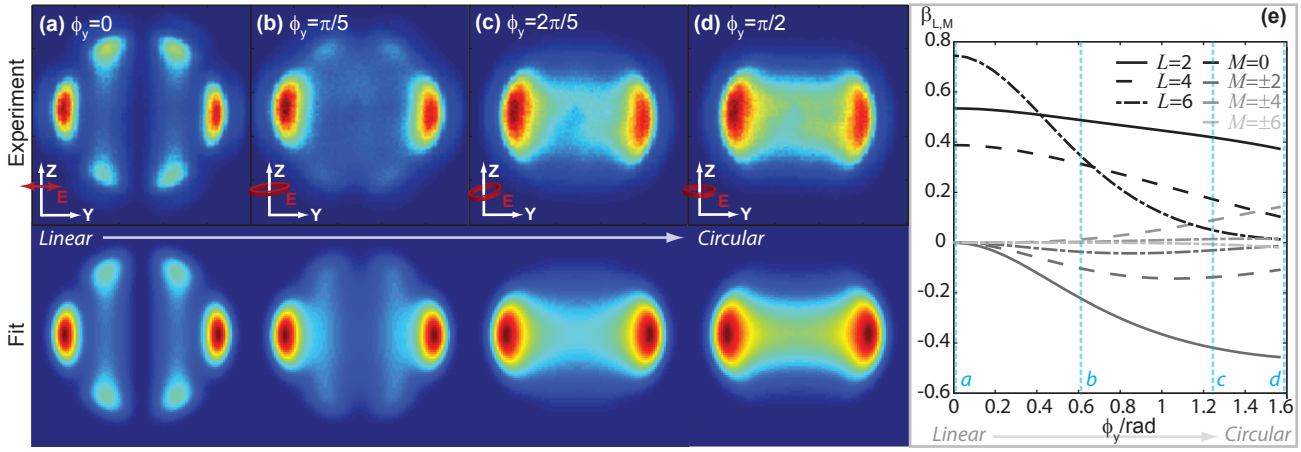


Figure 2. (a) - (d) raw data and fit result for the four polarizations investigated. The laser propagates along the $z$-axis and the polarization state, defined in the $(x, y)$ plane, is illustrated schematically as the polarization varies from linear (a) to circular (d); electrons are detected/integrated in the $(y, z)$ plane. (e) Calculated $\beta_{LM}$ parameters as a function of polarization ($\phi_y$), line styles denote $L$ and shading $M$. The polar axis for the $\beta_{LM}$ is chosen to match the $y$-axis in (a).

| Transition | | | $\lvert R_{l_1 l_2}\rvert$ | $\lvert R_{l_1 l_2}\rvert^2$/% | $\delta_{l_1 l_2}$/rad. |
|---|---|---|---|---|---|
| $l_1$ | | $l_2$ | | | |
| $i \to v$ | p | s | 0.34 (3) | 12 (4) | 0 * |
| | p | d | 0.94 (8) | 88 (11) | -1.62 (4) |
| $v \to f$ | s | p | 0.85 (8) | 72 (12) | -0.19 (3) |
| | d | p | 0.14 (2) | 2 (2) | -2.08 (8) |
| | d | f | 0.51 (9) | 26 (13) | 0.24 (7) |

Table I. Fitted values for the relative transition matrix element magnitudes, $|R_{ll}|$, and phases, $\delta_{ll}$. The square of the magnitudes is expressed as a percentage of the total transition amplitude, normalized to unity for each step (these percentages are also shown in figure 1). Uncertainties in the last digit are given in parentheses. * reference phase, set to zero during fitting.

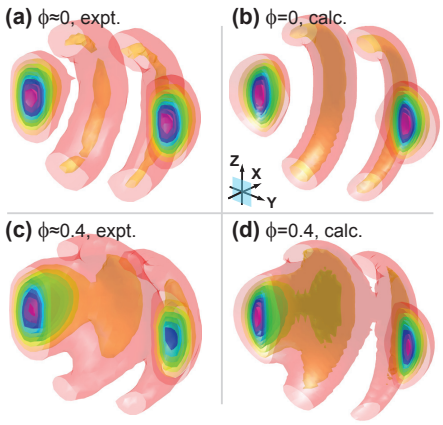


Figure 3. Tomographically reconstructed data & calculated distributions based on the fitted ionization matrix elements. The 3D distributions are sliced in order to reveal the radial distribution in detail; the nested isosurfaces run from 10% (pale red) to 90% (purple) density.

future publication [**?** ]. It is anticipated that, with the use of rich tomographic data-sets, the methodology discussed here may be applied to more complex systems, where a greater number of partial waves may play a role and 2D imaging data may not prove sufficient for robust analysis.

Finally, we illustrate the application of the ionization matrix elements determined above to the case of a more complex polarization-shaped pulse, shown in figure 4. For such polarization-shaped pulses, the PAD can be considered as a sum over the "basis states" given by the PADs correlated with individual polarization states, as defined by the $\beta_{LM}(\phi_y)$ expansion in figure 2(e); an experiment utilizing a polarization-shaped pulse thus constitutes a highly-multiplexed interrogation of the light-matter interaction in polarization space. Consequently the PAD may be highly structured, and is extremely sensitive to the exact shape of the laser pulse. The 2D projections may show even greater sensitivity to the pulse shape than the full $I(\theta, \phi)$ distribution, due to the enhanced effect of rotations of the distribution on the image plane projections; in this manner pulse shaping with imaging detection can lead to a wide range of 2D projections, even in the case where only a few partial wave channels are accessed in the ionization continuum.

In this work we have demonstrated the utility of complex intra-pulse light-matter interactions as a means to "complete" photoionization experiments, requiring only a few experimental measurements, combined with theoretical treatment of the intra-pulse dynamics, to obtain a set of ionization matrix elements. The validity of the radial matrix elements determined from the experimental data were further tested by comparison with tomographic (3D) data. In the case of potassium multiple pathways play a role at the 1 and 2-photon level, with $p \to d \to f$ the major ionization path. With the ionization matrix elements to hand calculations of the PAD for polarization-shaped laser pulses become possible, and this was illustrated for a specific spectral phase mask. This methodology is applicable to any arbitrarily shaped laser field, providing the ionization can be treated perturbatively and the photoelec-

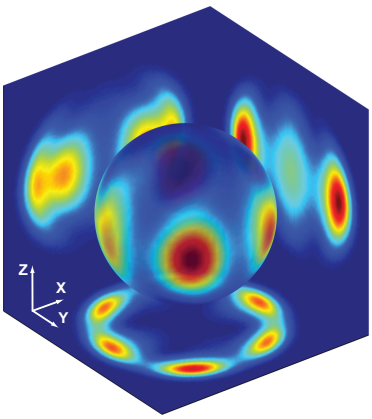


Figure 4. Application using a polarization shaped pulse. Calculated PAD for $E_{X,Y}(t)$ obtained by application of a $-\pi/2$ spectral phase mask to the red half of the spectrum, similar to the experimental pulses discussed in ref. [20]. The full $I(\theta, \phi)$ distribution is shown in spherical projection, along with 2D projections onto different Cartesian image planes.

tron energy spread is small (with respect to the response of $R(k)$), thus enabling a route to designing control fields with full understanding of the control process. Combined with tomographic reconstruction, or other means of obtaining full 3D PADs, this should be a powerful technique for understanding the ionization dynamics in many atomic systems, and should be extensible to molecular ionization dynamics, including multiphoton ionization of chiral molecules (which exhibits photoelectron circular dichroism [**? ?** ]) - provided that the population dynamics can be accurately modelled.

Acknowledgements: We thank Albert Stolow for suggesting this collaboration.

* Email: paul.hockett@nrc.ca

[1] K. L. Reid, Annual Review of Physical Chemistry **54**, 397 (2003), http://arjournals.annualreviews.org/doi/pdf/10.1146/annurev.physchem.54.011002.103814, http://arjournals.annualreviews.org/doi/abs/10.1146/annurev.physchem.54.011002.103814

[2] N. Cherepkov, Journal of Electron Spectroscopy and Related Phenomena **144-147**, 1197 (2005), ISSN 0368-2048, proceeding of the Fourteenth International Conference on Vacuum Ultraviolet Radiation Physics, http://www.sciencedirect.com/science/article/B6TGC-4FN76KF-C/2/6dd2efdee69724e71f409dfbdeb79f57

[3] U. Becker, Journal of Electron Spectroscopy and Related Phenomena **96**, 105 (1998), ISSN 0368-2048, http://www.sciencedirect.com/science/article/B6TGC-3WWCCJS-11/2/3a05a354364026bc5a2673c02b0849a9

[4] J. A. Duncanson, M. P. Strand, A. Lindgård, and R. S. Berry, Physical Review Letters **37**, 987 (Oct 1976)

[5] J. Hansen, J. Duncanson, R.-L. Chien, and R. Berry, Physical Review A **21**, 222 (Jan. 1980), ISSN 0556-2791, http://link.aps.org/doi/10.1103/PhysRevA.21.222

[6] R.-l. Chien, O. Mullins, and R. Berry, Physical Review A **28**, 2078 (Oct. 1983), ISSN 0556-2791, http://link.aps.org/doi/10.1103/PhysRevA.28.2078

[7] H. T. Duong, J. Pinard, and J. L. Vialle, Journal of Physics B: Atomic and Molecular Physics **11**, 797 (Mar. 1978), ISSN 0022-3700, http://iopscience.iop.org/0022-3700/11/5/013http://stacks.iop.org/0022-3700/11/i=5/a=013?key=crossref.14bdf0a8a61a010bca7afb8871505242

[8] P. Lambropoulos, Journal of Physics B: Atomic and Molecular Physics **6**, L319 (Nov. 1973), ISSN 0022-3700, http://stacks.iop.org/0022-3700/6/i=11/a=005

[9] O. Geßner, Y. Hikosaka, B. Zimmermann, A. Hempelmann, R. R. Lucchese, J. H. D. Eland, P.-M. Guyon, and U. Becker, Physical Review Letters **88**, 193002 (Apr 2002)

[10] M. Lebech, J. C. Houver, A. Lafosse, D. Dowek, C. Alcaraz, L. Nahon, and R. R. Lucchese, The Journal of Chemical Physics **118**, 9653 (2003), http://link.aip.org/link/?JCP/118/9653/1

[11] A. Yagishita, K. Hosaka, and J.-I. Adachi, Journal of Electron Spectroscopy and Related Phenomena **142**, 295 (2005), ISSN 0368-2048, modern Electron Spectroscopy of Atoms and Molecules. A collection of invited papers dedicated to Professor Katsumi Kimura in recognition of an esteemed research career spanning a 50-year period., http://www.sciencedirect.com/science/article/B6TGC-4DVW2XM-1/2/4200b83f67d15b8c407326659aed6d1d

[12] T. Suzuki, Annual review of physical chemistry **57**, 555 (Jan. 2006), ISSN 0066-426X, http://www.ncbi.nlm.nih.gov/pubmed/16599821

[13] Y.-I. Suzuki, Y. Tang, and T. Suzuki, Physical chemistry chemical physics : PCCP **14**, 7309 (May 2012), ISSN 1463-9084, http://pubs.rsc.org/en/content/articlehtml/2012/cp/c2cp40308k

[14] D. J. Leahy, K. L. Reid, and R. N. Zare, The Journal of Chemical Physics **95**, 1757 (1991), http://link.aip.org/link/?JCP/95/1757/1

[15] K. L. Reid, D. J. Leahy, and R. N. Zare, Physical Review Letters **68**, 3527 (Jun 1992)

[16] P. Hockett, M. Staniforth, K. L. Reid, and D. Townsend, Physical Review Letters **102**, 253002 (Jun 2009)

[17] Z.-M. Wang and D. S. Elliott, Physical Review Letters **87**, 173001 (Oct 2001)

[18] Y.-Y. Yin, D. S. Elliott, R. Shehadeh, and E. R. Grant, Chemical Physics Letters **241**, 591 (1995), ISSN 0009-2614, http://www.sciencedirect.com/science/article/B6TFN-3YCN3B1-BR/2/9cf94c712099f5fa63e68636678babed

[19] Y.-Y. Yin, C. Chen, D. S. Elliott, and A. V. Smith, Physical Review Letters **69**, 2353 (Oct 1992)

[20] M. Wollenhaupt, M. Krug, J. Köhler, T. Bayer, C. Sarpe-Tudoran, and T. Baumert, Applied Physics B **95**, 245 (Feb. 2009), ISSN 0946-2171, http://www.springerlink.com/index/10.1007/s00340-009-3431-1

[21] M. Krug, T. Bayer, M. Wollenhaupt, C. Sarpe-Tudoran, T. Baumert, S. S. Ivanov, and N. V. Vitanov, New Journal of Physics **11**, 105051 (Oct. 2009), ISSN 1367-2630, http://stacks.iop.org/1367-2630/11/i=10/a=105051?key=crossref.55de25b7e39010381345e239f559aee3

[22] M. Wollenhaupt, C. Lux, M. Krug, and T. Baumert, Chemphyschem : a European journal of chemical physics and physical chemistry **14**, 1341 (May 2013), ISSN 1439-7641, http://www.ncbi.nlm.nih.gov/pubmed/23526773

[23] M. Wollenhaupt, a. Präkelt, C. Sarpe-Tudoran, D. Liese, and T. Baumert, Journal of Optics B: Quantum and Semiclassical Optics **7**, S270 (Oct. 2005), ISSN 1464-4266, http://stacks.iop.org/1464-4266/7/i=10/a=010?key=crossref.180ce4ecce2f16a3c633bd4778e66be0

[24] M. Wollenhaupt and T. Baumert, Faraday Discussions **153**, 9 (2011), ISSN 1359-6640, http://xlink.rsc.org/?DOI=c1fd00109d

[25] M. Wollenhaupt, M. Krug, J. Köhler, T. Bayer, C. Sarpe-Tudoran, and T. Baumert, Applied Physics B **95**, 647 (Apr. 2009), ISSN 0946-2171, http://www.springerlink.com/index/10.1007/s00340-009-3513-0

[26] A. Präkelt, M. Wollenhaupt, A. Assion, C. Horn, C. Sarpe-Tudoran, M. Winter, and T. Baumert, Review of Scientific Instruments **74**, 4950 (2003), http://scitation.aip.org/content/aip/journal/rsi/74/11/10.1063/1.1611998

[27] *Imaging in Molecular Dynamics: Technology and Applications*, edited by B. J. Whitaker (Cambridge University Press, Cambridge, 2003)

[28] C. Smeenk, L. Arissian, a. Staudte, D. M. Villeneuve, and P. B. Corkum, Journal of Physics B: Atomic, Molecular and Optical Physics **42**, 185402 (Sep. 2009), ISSN 0953-4075, http://stacks.iop.org/0953-4075/42/i=18/a=185402?key=crossref.901cc2b6043bd31df089e38d13fcd599

[29] P. Hockett, M. Staniforth, and K. L. Reid, Molecular Physics **108**, 1045 (Apr. 2010), ISSN 0026-8976, http://www.tandfonline.com/doi/abs/10.1080/00268971003639266

[30] M. Wollenhaupt, A. Assion, O. Bazhan, C. Horn, D. Liese, C. Sarpe-Tudoran, M. Winter, and T. Baumert, Phys. Rev. A **68**, 015401 (Jul 2003), http://link.aps.org/doi/10.1103/PhysRevA.68.015401

[31] In the calculations shown here $\delta_{\pm 1} = 0.05$ rad/fs, but for the same reason this value has no effect on the PADs, except as a scaling factor, in this case. For completeness, we also note that spin is neglected in this treatment.

[32] E. P. Wigner, Physical Review **98**, 145 (1955)

[33] We note for completeness that because the Wigner delay is the energy-derivative of the scattering phase it is not defined in absolute terms by a single-energy relative phase, but relative emission times may be determined from a set of such results.

[34] P. R. Bevington and D. K. Robinson, *Data Reduction and Error Analysis for the Physical Sciences*, 2nd ed. (McGraw-Hill, New York, 1992)

[35] B. Schmidtke, M. Drescher, N. a. Cherepkov, and U. Heinzmann, Journal of Physics B: Atomic, Molecular and Optical Physics **33**, 2451 (Jul. 2000), ISSN 0953-4075, http://stacks.iop.org/0953-4075/33/i=13/a=306?key=crossref.ec62c50a4abb6a8ccb8209c7b3c89478

[36] S. Ramakrishna and T. Seideman, Journal of Physics B: Atomic, Molecular and Optical Physics **45**, 194012 (Oct. 2012), ISSN 0953-4075, http://stacks.iop.org/0953-4075/45/i=19/a=194012?key=crossref.68faa78abc832ed11020afde085ac486

[37] C. Lux, P. Hockett, M. Wollenhaupt, and T. Baumert, In preparation(2014)